Nanoscale

Accepted Manuscript

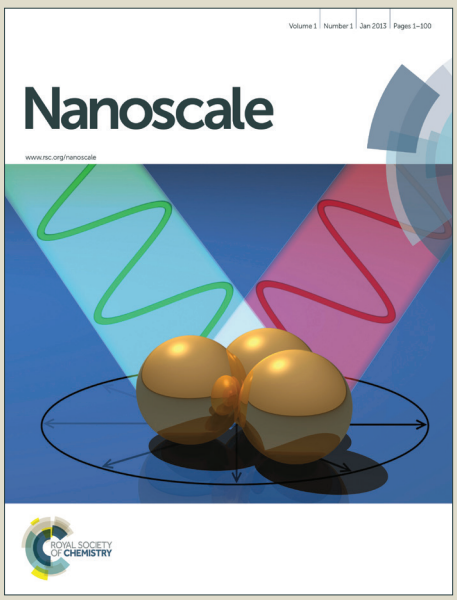

ROYAL SOCIETY OF CHEMISTRY

www.rsc.org/nanoscale

Nanoscale

Paper

Exploration of graphene oxide as intelligent platform for cancer vaccine†

Received 00th January 20xx,
Accepted 00th January 20xx

DOI: 10.1039/x0xx00000x

www.rsc.org/

Hua Yue,‡[a] Wei Wei,‡[a] Zonglin Gu,‡[b] Dezhi Ni,[a] Nana Luo,[a] Zaixing Yang,[b] Lin Zhao,[b] Jose Antonio Garate,[c] Ruhong Zhou,*[b,c,d] Zhiguo Su*[a,e] and Guanghui Ma*[a,e]

We explored an intelligent vaccine system via facile approaches with both experimental and theoretical technique based on the two-dimensional graphene oxide (GO). Without extra addition of bio/chemical stimulators, the microsized GO imparted various immune activation tactics to improve the antigen immunogenicity. A high antigen adsorption was acquried, and the mechanism was revealed to be a combination of electrostatic, hydrophobic, and π-π stacking interactions. The "folding GO" acted as a cytokine self-producer and antigen reservoir and a particular autophagy, which efficiently promoted the activation of antigen presenting cells (APCs) and subsequent antigen cross-presentation. Such a "One but All" modality thus induced high level of anti-tumor responses in a programmable way and resulted in an efficient tumor regression in vivo. This work may shed light on the potential use of new dimensional nano-platform in the development of high-performance cancer vaccines.

Introduction

Although chemotherapy and radiotherapy are first-line options for tumor treatment, they are usually associated with poor specificity and serious side effects.[1,2] Therefore, novel therapeutic strategies for efficient tumor suppression with less toxicity are urgently awaited. Cancer vaccines that can activate the power of patients' own immune system offer a big hope of controlling cancers with few side effects.[3,4] However, there are additional challenges to develop vaccine-based therapies, including unsatisfied cell recruitment, inefficient antigen delivery, or weak tumor killing. To circumvent these consecutive obstacles in the crucial steps for anti-tumor response, various immune activating tactics have been exploited. To recruit more functional antigen presenting cells (APCs, e.g. dendritic cells DCs or macrophages) to the vaccination sites, one popular tactic is co-administration of exogenous immunostimulatory cytokines/chemokines (e.g. granulocyte-macrophage colony-stimulating factor and interleukin IL-6) with antigen.[5] Following vaccination, to avoid rapid body clearance, delivering the antigens through micro/nano-particles (MP/NPs, which develop rapidly in the biomaterials field [6,7]) promises compelling advantages. In addition, particles can be grafted with APCs targeting ligands (e.g. mannose ligands and DEC 205 antibody) and carry more antigens into the APCs for further process.[8,9] As the subsequent antigen processing way determines the polarization of T cell immune response, current vaccines for tumor therapy predominantly focus on cross-presenting antigen to activate the CD8 cytotoxic T cells (CTL) for tumor killing. Corresponding strategies include fine-tuning the intracellular fate of MP/NP via particle functionalization or targeting specific Toll-like receptors (TLRs) via the help of danger signals (e.g. CpG oligonucleotides).[10,11]

Nevertheless, the performances of the aforementioned tactics are still less than expectation, as each one merely pinpoints an individual session. In this case, only if the vaccine platform integrates all the capacities (APCs recruitment/activation, antigen delivery, and cross-presentation) into one entity, can the best antitumor efficacy be achieved. Toward this end, studies have attempted to join these tactics into a single vaccine platform, resulting in the rising of MP/NP-based "All in One" vaccines.[12] Albeit promising, such a vaccine platform poses new formidable challenges. On one hand, harsh preparation conditions and complex control process are required for its construction. On the other hand, these different tactics often act separately or non-sequentially and barely functions in a programmable fashion, thus compromising the antitumor efficacy. Therefore, a novel vaccine platform that could integrate these capacities

[a]*National Key Laboratory of Biochemical Engineering, Institute of Process Engineering, Chinese Academy of Sciences, Beijing 100190, China. E-mail: ghma@ipe.ac.cn; zgsu@ipe.ac.cn.*
[b]*Institute of Quantitative Biology and Medicine, SRMP and RAD-X, Collaborative Innovation Center of Radiation Medicine of Jiangsu Higher Education Institutions, and Jiangsu Provincial Key Laboratory of Radiation Medicine and Protection, Soochow University, Suzhou 215123, China*
[c]*Computational Biology Center, IBM Thomas J. Watson Research Center, Yorktown Heights, NY 10598, USA*
[d]*Department of Chemistry, Columbia University, New York, NY 10027, USA. E-mail: ruhongz@us.ibm.com*
[e]*Collaborative Innovation Center of Chemical Science and Engineering (Tianjin), Tianjin 300072, China*
†Electronic Supplementary Information (ESI) available: See DOI: 10.1039/x0xx00000x
‡These authors contributed equally to the work

in a facile way and act in a programmatic pattern is highly expected.

Recently, the two-dimensional (2D) material graphene oxide (GO) has received extensive interests due to its extraordinary attributes, and great efforts have been exerted in the diagnostics and therapeutic field.[13-16] Nevertheless, further employment of the graphene-mediated vehicle is still calling for deeper mechanistic understanding of interaction between GO and bio-system. In one of our previous systematic study, we found that GO exhibited intriguing biological effects at the cellular level.[17] In detail, GO (without any modification) were prone to be internalized by macrophages rather than by non-phagocytes. Furthermore, GO at micro size was superior to the nano size in the upregulation of immune activation cytokines. Moreover, GO was trafficked through a specific cellular pathway, which might be intimately linked with the presentation pathway. Although the study was evaluated on macrophages (one type of APCs), it hinted that GO might have the capacities to display multiple roles that desired for the novel vaccine platform.

Inspired by the proved merits, we formulated GO with OVA (ovalbumin, a well-documented antigen model for both experimental and mechanistic study) and systematically examined its immunotherapy effect against cancer. This vaccine formulation was constructed by using a facile mixing/adsorption approach without chemical coupling or ligand functionalization, which excluded antigen inactivation during complicated formulation process and ensured more repeatable results. After deeply understanding the mechanism of antigen loading on GO via computational simulations, the programmed boosts of GO on consecutive immune activation were investigated in bone marrow dendritic cells (BMDC, primary professional cells for antigen presenting). In the in vitro evaluation, we found a particular GO-triggered autophagy pathway that account for the enhancement of antigen cross-presentation. Based on this groundwork, we tested the in vivo adjuvant efficacy of GO by employing OVA specific transgenic mice (OT-1) and verified the therapeutic effects in E.G7-OVA tumor-bearing mice. Present work unveiled an intelligent vaccine modality under the extensive exploration of the intrinsic attributes of GO, shedding light on an immunotherapy approach against cancer.

Experimental

Synthesis and characterization of GO.

Preparation of uniform-sized sheets was started from the primary GO made by a modified Hummers method. After sufficient sonication and a washing process for Mn removal, the 2 μm GO sheets were separated by a centrifugal force of 100-200 g as previously published.[17] To prepare the GO-antigen formulation, 100 μg GO were added to the soluble OVA, and the GO-OVA formulation at a desired concentration of NP/antigen was acquired by a facile mixing/adsorbing process at 37 °C for 2 h. The adsorbed protein amount was assayed by the Bicinchoninic acid (BCA) Kit. Atomic force microscopy (AFM) analysis of GO-OVA formulation was primarily performed on a BioScope Catalyst atomic force microscopy (Veeco). To determine the thickness of the protein that adsorbed on GO, the height analysis was carried out. To clarify the OVA adsorption event, we monitored the fluorescent and UV-Vis absorb spectrum during GO-OVA interaction process by using Infinite M200 spectrophotometer (Tecan).

Molecular dynamics (MD) simulation methods.

GO was constructed upon the Lerf–Klinowski structural model with a molecular formula of $C_{10}O_1(OH)_1$ in the absence of the carboxylic acids on the periphery of the basal plane of the graphitic platelets of GO. OVA (PDB ID 1OVA) was composed by four homologous chains forming a centrosymmetric structure. Following similar protocols as in our previous studies,[18-20] we included both GO and OVA in the simulation system, with the initial minimum distance between OVA and GO set to be 1.0 nm, in which GO was constrained during the simulation. The simulation box has a size of 11.36 nm×15.34 nm×16.24 nm, which contained a total of 274,122 atoms. All the MD simulations were carried out on a Linux cluster using the software package GROMACS (version 4.6.6) with GROMOS 54 a7 force field. The temperature and pressure were set to 300 K and 1 bar, respectively. The long-range electrostatic interactions were treated by PME (Particle Mesh Ewald), while a typical smooth cutoff was used for the van der Waals interactions, with a cutoff distance of 10 Å. The simulation length was set for 100 ns for all the five trajectories run.

Determination of GO-induced autophagy.

To image the autophagy phenomenon induced by GO, BMDC were seeded in petri dish at the initial density of 1×10^6 cells/well. GO was added at a concentration of 5 μg/mL or 20 μg/mL, respectively. Cells that treated with rapamycin (autophagy inducer) were used as positive control. After GO treatment, cells were fixed in 3.7% (v/v) formaldehyde and permeabilized with 0.2% (v/v) Triton X-100 at room temperature. Subsequently, samples were blocked with 5% (v/v) goat serum and incubated with rabbit anti-murine Beclin 1 and LC3 A/B antibody at 4 °C for 24 h. The staining was performed with Alexa Fluor 488-labeled goat anti-rabbit Ab and DyLight 549 goat anti-rabbit IgG Ab at room temperature for 30 min, respectively. Corresponding fluorescent images at 500-560 nm and 650-700 nm were taken by the UltraView VoX (PerkinElmer).

In vitro assay of antigen adjuvanticity of GO.

BMDC were seeded in 24-well plate, challenged with OVA or GO-OVA for 12 h and then post cultured for 0, 24 and 48 h. Surface molecules of antigen presenting cells (APCs) including costimulator CD86, recognition signal MHC II, and OVA specific MHC I were stained with corresponding fluorescence-conjugated antibody at 4 °C for 0.5 h. Relative expressions of cell molecules were analyzed on flow cytometry (FACS). (Similar assay were performed to investigate the antigen presenting signals on lymph node DC after 48 h vaccination.) To monitor the cytokine profile of the DCs, cell culture

supernatants were collected, and the secretion levels of IL-6, IL-12, TNF-α, MCP-1, and IFN-γ were detected using a Cytometric Bead Array (CBA) Mouse Inflammation Kit (BD) and FACS analysis according to the manufacturer's instructions.

In vivo imaging of OVA injected mice.

To test the antigen preservation effect of GO, the mice were injected intravenously with Cy5-labeled OVA formulations. At different time intervals, the mice injected with OVA and GO-OVA were anesthetized and scanned using an in vivo imaging system (FX Pro, Carestream) with an excitation band pass filter at 633 nm and an emission filter at 670 nm.

FACS analysis of immune effector cells in antigenic immunized mice.

Lymph nodes, spleens and tumors were harvested from the immunized mice. Lymph nodes and spleens were torn apart into single cell suspensions by pressing with plunger of a syringe, while resected tumors were minced into sections of approximately 3 mm and digested by 175 U/mL of Collagenase IA (supplemented in RPMI media). All the resulting cell suspensions were stained with PerCP-Cy5.5-CD3 and PE-Cy7-CD8α Abs for 30 min at 4 ^{o}C. The CD3 and CD8-positive subset of T cells were investigated by FACS.

CTL cell proliferation induced by GO-OVA.

The in vivo proliferation of OVA-specific CD8 T was measured by a carboxyfluorescein diacetate succinimidyl ester (CFSE) dye dilution assay. Briefly, OT-1 CD8 T enriched by Dynal CD8 negative isolation kit were stained with 0.5 μM CFSE. The separated labeled OT-1 T cells (2×10^6) were intravenously injected into the C57BL/6 recipients. These mice were immunized with different formulations 12 h later. After an additional 60 h, splenocytes were isolated and stained with PerCP-Cy5.5-CD3 and PE-Cy7-CD8α mAbs. The division of OVA-specific CD8 T was analyzed by FACS analysis of CFSE dilutions.

Cytotoxicity activity of CTL induced by GO-OVA.

To evaluate antigen-specific CTL activity, single-cell suspensions from the pooled spleens (n=3) of immunized mice were isolated 14 days after the antigenic injection. Splenocytes were restimulated with SIINFEKL (OVA specific MHC I) peptide for 3 days in PRIM 1640 medium containing 20 U/mL recombinant IL-2. Subsequently, these activated effector cells were mixed with mitomycin-treated E.G7 cells or EL-4 target cells. The CTL activity was evaluated at various ratios of effector cells to target cells (E/T ratios) in a Lactate dehydrogenase (LDH) cytotoxicity detection assay. To assess the proportion of IFN-γ^+ CD8 T, the splenocytes were stimulated ex vivo with 5 μg/mL SIINFEKL for 6 h. The cells were then fixed, permeabilized, stained with anti-IFN-γ and anti-CD8α, and analyzed by FACS.

Tumor-bearing mice and therapy study.

The main text of the article should appear here with headings as appropriate. Mice were randomly assigned to different groups (n=7 for each group). To establish tumor models, E.G7 cells (2×10^6) were injected into the left axillary region of the C57BL/6 mice on day 0. Vaccines were subcutaneously injected into the lower right flank. In each group, 20 μg soluble OVA or an equivalent dose of OVA loaded on GO was used for the GO-OVA group. The immunization for GO-OVA group was given on day 5, when the tumor was palpable, and a boost immunization was administered for the GO-OVA 2 group on day 10. To monitor tumor progression, tumor sizes were measured continually and represented as $1/2\times L\times W^2$ (mm^3), where L is the longest and W is the shortest tumor diameter. The tumor volumes of deceased mice were not included after the day of death.

Results and discussion

Ultra-high antigen adsorption efficiency of the 2D GO

Prior to the preparation of the antigen formulation, Mn removal pretreatment was carried out to avoid any hazards of residual metal sourced from the GO preparation according to our previous study,[17] and the well distributed GO sheets (with ~2 μm diameter and 4 nm height) were obtained for antigen loading (Fig. S1†). After a simple adsorption/mixing protocol, the adsorption ratio of OVA:GO reach up to 5:1 (w/w) within only 1 h (Fig. 1a and S2†). The efficient adsorption was evident from the increased UV-Vis absorption at 280 nm (Fig. 1b) and the sharp declination of the intrinsic OVA fluorescence (Fig. 1c). In further AFM analysis, the zoomed picture also provided straightforward evidence that OVA antigens were compactly adsorbed onto the GO surface in an ovoid morphology (Fig. 1d). Compared with the height of pristine GO (~4 nm), the average thickness of OVA loaded GO jumped up to ~25 nm (Fig. 1e). As the diameter of the OVA protein is around 4 nm, we proposed

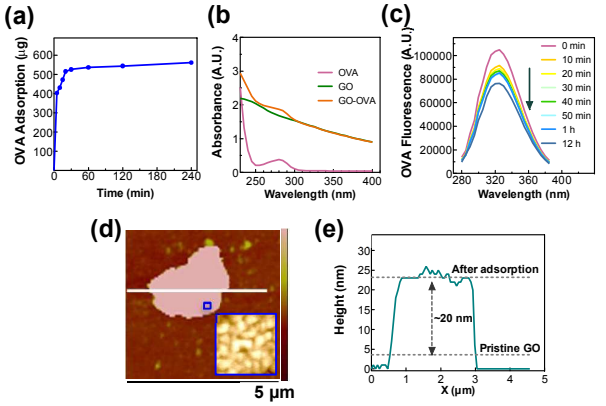

Fig. 1. Characterization of the ovalbumin (OVA)-loaded Graphene oxide (GO). (a) Adsorption kinetics of OVA on GO (100 μg). (b) UV-Vis absorption curves of GO before and after OVA loading. (c) Fluorescence spectrum of OVA (at the 230 nm excitation wavelength) before (0 min) and after adsorption on GO. Atomic force microscopy height images (d) and corresponding height analysis (e) of the GO after loading OVA.

The insert is a zoomed graph from the indicated image square (200 nm×200 nm).

that multilayered antigen adsorption could occur onto the GO surface. Such a high loading efficiency was expected to decrease the amount of exogenous carrier GO, minimizing the possibility of unexpected side effect. Meanwhile, the demand of antigen also decreased owing to the high efficiency, which was particularly desired for vaccines that under limited antigen resource.[21,22]

Simulation of GO-OVA interaction

To elaborate the adsorption process, we performed all-atom molecule dynamics (MD) simulation for a system consisting of the OVA protein and GO material (see Fig. S3† for the system setup) following similar protocols in our previous studies.[18-20] As shown in Fig. 2a for one representative trajectory, the charged amino acid residues played the most important role at the equilibrium state. The contact number between the charged residues and GO was up to ~1730, followed by the hydrophilic residues (~1220), hydrophobic residues (~1110), and aromatic residues (~320). Clearly, compared with other residues, there are plenty number of charged and hydrophilic residues existing on the OVA's surface. In a very recent study, Stauffer et al.[23] have shown that the adsorption energies between the twenty different types of amino acids and the heavily oxidized GO surface have no significant differences (-0.35 ~ -0.62 eV per residue, with Trp and Arg showing the strongest interaction energies, consistent with our own previous findings[18]). It suggested that the local complex nature of the GO surface (hydrophobic aromatic rings plus hydrophilic oxidized groups) could smooth out the differences in the amino acid types in terms of the interaction energies. Therefore, we could attribute the strong GO-OVA interaction mostly to the charged and hydrophilic residues on the OVA protein surface. Meanwhile, we found that the van der Waals (vdW) interaction, as low as -243.23 kcal/mol, also contributed significantly to the binding between OVA and GO (similar to the cell membrane/GO interaction[19]), along with the hydrogen bonding between OVA and oxidized groups on GO, which had a mean value of ~3.75 at the equilibrium state (Fig. 2b). In addition, the π-π stacking interaction between the aromatic residues and the GO surface carbon rings can contribute up to -6 ~ -13.5 kcal/mol for each pair,[24] which was also shown to play a significant role in graphene's binding with other proteins.[25,26] Thus, the adsorption process of OVA onto GO was a result of a complex interplay among all the interactions involved, electrostatic, hydrophobic, hydrogen bonding, as well as π-π stacking interactions.

To further illustrate these important interactions, in particular the more specific π-π stacking and hydrogen bonding interactions between OVA and GO, representative local snapshots are shown to capture a tyrosine and glutamine residue in action. From Fig. 2c, we found that when the tyrosine (Tyr111) approached closer to GO, its head hydroxyl group in the side chain contacted the hydrophilic hydroxyl and epoxy groups of GO, while its aromatic ring packed with the "pure" graphene (the "sp2 domain" of the GO[27-29]). The overall structure formed a "face-to-face" configuration with graphene, which was recognized as a more stable structure

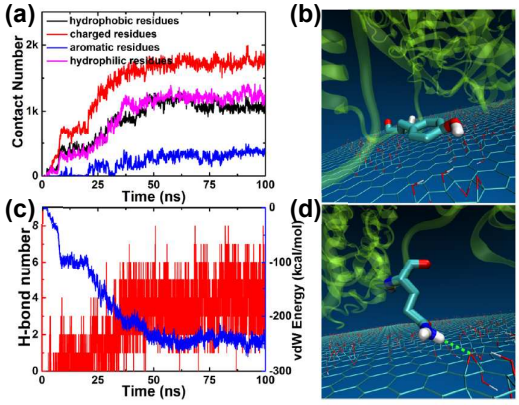

Fig. 2. Heavy atom contact number of hydrophobic (black), charged residues (red), aromatic residues (blue) and hydrophilic neutral residues (magenta) (a), the vdW energy (blue curve) and hydrogen bond number (red curve) between OVA and GO (b), and the local snapshots showing the π-π stacking interaction (tyrosine) (c) and hydrogen bond interaction (glutamine) (d).

with lower interaction energy previously.[24] On the other hand, as shown in Fig. 2d, the glutamine residue (Gln169) pointed its polar side chain towards GO to form a hydrogen bond between its –NH2 group and the epoxy group on GO in this case. These atomic detailed and specific interactions provide a deeper understanding on the interactions between the OVA protein and GO (which can also be seen in the vivid movie).

The role of GO in antigen reservoir and autophagy induction

Next, we prepared the GO-OVA formulation and investigated the role of GO in delivering antigen to APCs and the intracellular presentation. The FACS data showed that the OVA uptake by BMDC at 12 h was significantly improved (to ~2.5 fold) with the assist of GO carrier (Fig. 3a). After replacing the antigen formulation with fresh medium for post incubation, the level of residual antigen at 48 h in cells sharply decreased to 15% of the maximum internalization in OVA group. In contrast, a relatively high level was maintained for the GO-OVA group under the same procedure. The improved antigen uptake and slower attenuation pointed towards the role of GO as an "antigen reservoir". When in close contact to the cells, GO could directly insert into the cell membrane (Fig. S4†), and thus GO-OVA was more inclined to traffic through a direct cytoplasmatic pathway (as indicated by free green spots in the overlay image of Fig. 3b). In contrast, antigens were highly sequestered in lysosomes for OVA group, with the subsequent degradation carried out by the inner acidic enzymes. We also noticed that the original flat GO (Fig. S5†) stacked and shifted

toward a folded morphology (indicated by red stars in Fig. 3C). This phenomenon explained the reservoir behavior of GO, as it would wrap the antigens in the wrinkles, protecting them from rapid degradation by the intracellular enzymes.

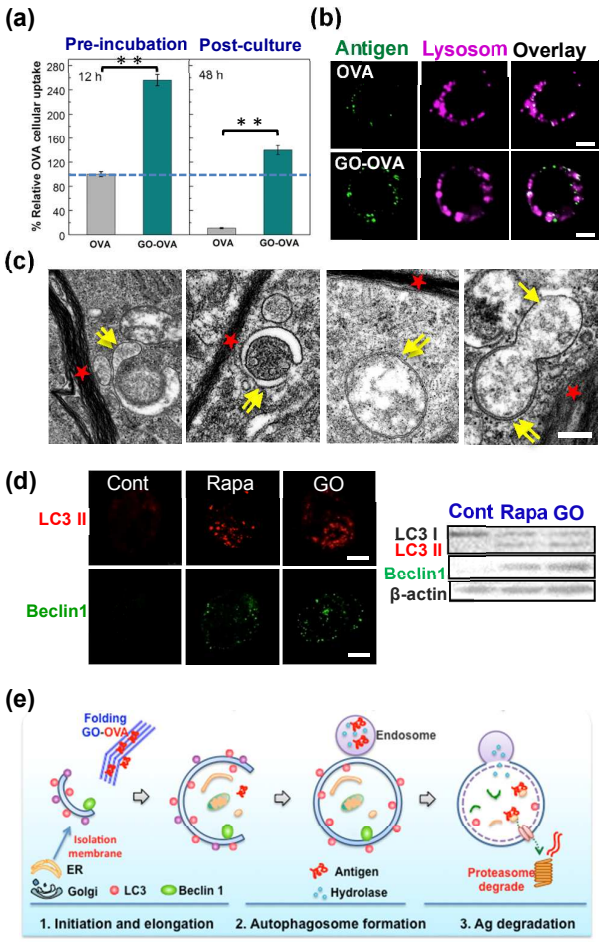

Fig. 3. Multifunctional role of GO in superior antigen uptake, trafficking and autophagy mediated antigen presentation in bone marrow dendritic cells (BMDC). (a) Flow cytometry (FACS) data showing the improved OVA internalization in BMDC with or without the assistant of GO after 12 h OVA pre-incubation and 48 h post-culture period. (b) The dual trafficking pathway of GO-OVA in both lysosomes and cytoplasm, in comparison with the sole lysosomal trafficking of pure OVA in BMDC. The colocalization information of antigen (green) and lysosomes (purple) were indicated by white spots. Scale bars, 5 μm. (c) Transmission electron microscopy images of autophagy procedure underwent by the GO-pulsed DCs. Typical double-membrane autophagosomes (indicated by double-head arrows) were found in GO (indicated by red stars) treated BMDC. Scale bars, 200 nm. (d) Confocal images (left panels) and corresponding western blot data (right panels) showing the expression of autophagy related protein in untreated, rapamycin (rapa, autophagy inducer) treated, and GO (5 μg/ml) treated BMDC for 12 h. Scale bars, 5 μm. (e) Schematic diagram of autophagy effect induced by GO. Data represent the mean±s.d. (n=3, *p<0.05, **p<0.01).

More importantly, we clearly unveiled an intriguing autophagy event of cells after exposure to GO. Upon the folding of GO, the “bowl” like phagophores (indicated by double yellow arrows, Fig. 3c) with typical two-layered membrane emerged and prolonged, followed by enclosure of organelles and formation of intact orbicular autophagosomes. The outer autophagosome membrane was then ready to fuse with monolayer endosome/lysosome (as indicated by single yellow arrow), where the exogenous substances could be degraded by the protease that simultaneously enclosed in this vesicle. To clarify the initiation mechanism, the autophagy-associated proteins were determined by immunofluorescence analysis and western blot (Fig. 3d and S6†). The involvements of Beclin 1 and membranous LC3-II punctuates (conversed from soluble LC3 I) were confirmed, as both of their expressions were upregulated in the GO group (at either 5 or 20 μg/mL concentration), similar to the outcome of the rapamycin group (autophagy positive control). In addition to the possible molecular pathway (TLR4/TLR9 regulated way),[30] the stress response against the "folding GO" was demonstrated another crucial mechanism for the autophagy.

According to the aforementioned data, we depicted a schematic view and opened up the interaction scenario of cells when they came across GO (Fig. 3e). With the assistance of the GO insertion, a large amount of antigens were capable of directly entering the cytoplasm. The folded GO then acted as antigen reservoir and induced autophagy through Beclin 1 and LC3 II mediated pathway. In this case, antigens that released from the wrapped GO were prone to fuse with the autophagosomes created at the end. It was worth mentioning that autophagy has been demonstrated to link with antigen cross-presentation.[31-33] In virtue of the preferred intracellular trafficking as well as GO induced autophagy s, antigens were more likely to be cross-presented to the CD8 T cells.

In vitro adjuvanticity of GO

The favorable performance of GO on the intracellular fate of antigen enlightened us to validate its effects on the APCs presentation. Being similar to the expression of costimulator CD86, the MHC II molecule level was obviously upregulated in the GO-OVA group in comparison with those in the OVA group (Fig. 4a and b). As MHC II is ordinary for exogenous antigen, above upregulations were mainly ascribed to the larger amount of antigens that ferried by GO. Notably, OVA specific MHC I level was dramatically elevated under GO-OVA challenge, comparing with negligible change observed in the OVA group (Fig. 4c). As the MHC I peptide complex offers recognition information to CD8 T,[34] the behavior seen with GO-OVA validated the bonus of the aforementioned intracellular trafficking and autophagy induction on antigen cross-presentation. Furthermore, the reservoir role of GO offered a benefit to keep the T activation signals (including MHC I, MHC II and CD86) presenting on cell surface over 48 h.

Such durable presentations were considered to endow the APCs with more opportunities to prime specific immune response.[35]

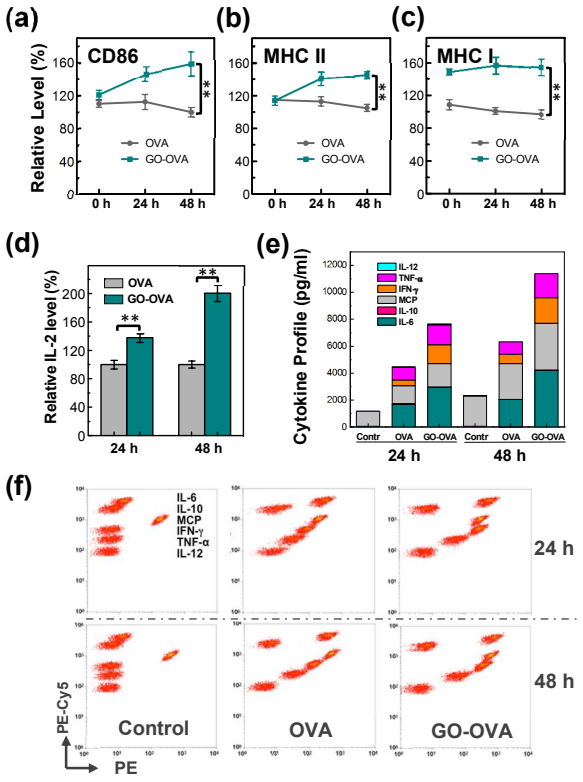

Fig. 4. The in-vitro adjuvanticity of GO in APCs activation and T cell priming. Upregulated and prolonged presentation of CD86 (a), MHC II (b), and OVA specific MHC I (c). Cells were pre-incubated with OVA or GO-OVA for 12 h and then post-cultured for 0, 24 and 48 h. GO-OVA treated BMDC not only highly presented MHC II for CD4 T cell recognition but also upregulated the OVA specific MHC I (SNIIFKL) for CD8 T cell recognition. (d) Relative expression of proliferative signal IL-2 of CD8 T after incubation with antigen pulsed BMDC. FACS histogram (e) and dot plots (f) showing the cytokine profile of the antigen-challenged BMDC at different coincubation (BMDC-CD8 T) time. Data represent the mean±s.d. (n=3, *p<0.05, **p<0.01).

Apart from the antigen presentation, a profile of self-produced cytokines related to the immune regulation and activation was evaluated. Upon 48 h incubation with GO-OVA pulsed BMDC, CD8 T produced significantly larger amount of IL-2 (200% of that in OVA group), which was favorable for the T cell proliferation (Fig. 4d). In addition, GO-OVA induced APCs to secrete higher levels of IL-6 and monocyte chemotactic protein 1 (MCP-1), which could function as attractants to allure more APCs. Meanwhile, immune activators (e.g. IL-12 and IFN-γ) rather than immune suppressors (e.g. IL-10) were also produced (Fig. 4e and f). The GO acted as a cytokine promoter to further enhance APCs activation/recruitment and T cell proliferation.

In vivo APC activation and CTL response

To clarify whether the GO based vaccine remains functional in an animal model, we investigated the in vivo fate of different antigen formulations. After subcutaneous injection of the soluble OVA (Cy5 labeled) in the hindneck of C57BL/6 mice, the antigen signal remarkably decayed to 10% from the initial response within 3 h (Fig. 5a). In contrast, the deposited antigen signal in GO-OVA group remained for a much longer period (~20% residual at 24 h). As GO-OVA induced APCs to self-produce large quantities of recruiting cytokines (IL-6 and MCP-1), patrolling APCs could be recruited in time via communicating with APCs near the injection site (Fig. 5b). The durable antigen persistence in GO-OVA group thus prolonged temporo-spatial coexistence of antigen and cell, which enhanced the probability of APCs to utilize the OVA inside the local "antigen arsenal". Following efficient antigen delivery and extensive antigen processing, the APCs expressed higher levels of T activation signals (especially for MHC I) in the lymph node (Fig. 5c), which thus provided supporting evidence towards the proliferation and activation of CD8 T.

In order to assess the CTL multiplying issue, OVA specific CD8 T cells from the transgenic OT-1 mice and a CFSE fluorescence dilution protocol were employed. Comparing with a marginal effect in OVA group (16%) (Fig. 5d), the antigen specific CD8 T cells dramatically proliferated (a rise of 79% fluorescence dilution) under the adjuvanticity of GO. With the preferred cell multiply of CD8 T cells (CTL), their functions including cytokine production and cytotoxic lysis were expected. We observed that the frequency of IFN-γ secreting CD8 T cells increased eight-fold above the control cells (Fig. 5e), in contrast to a feeble increase in the OVA group. In addition, prominent CTL responses against the OVA-expressing target cells (E.G7) were induced after 14 days of immunization with GO-OVA formulation, whereas no significant lysis activity was detected in the negative control cells (EL-4, the pristine cell type without OVA gene) (Fig. 5f). This result suggested an effective and specific clearance of antigen positive targets.

Tumor therapy effect in the E.G7-OVA thymoma model

Encouraged by the in vitro potential, we next evaluated the antitumor performance of GO-OVA formulation in an E.G7 tumor-bearing mice model. Compared with that of the PBS or OVA control group, the tumor growth was significantly suppressed in GO-OVA group (Fig. 6a and c). When the mice were given a boost immunization (GO-OVA 2) on day 10, the tumor growth was under a more significant restriction, and the tumor volume decreased 80% (below the OVA group) on day 21. A greatly prolonged survival time was correspondingly achieved for the GO-OVA group (Fig. 6b). Countering to no survival in the OVA group, only one mouse had died until day 28. We also noticed obvious tumor lysis cavities in the GO-OVA groups rather than in the OVA or control groups (Fig. 6d) when

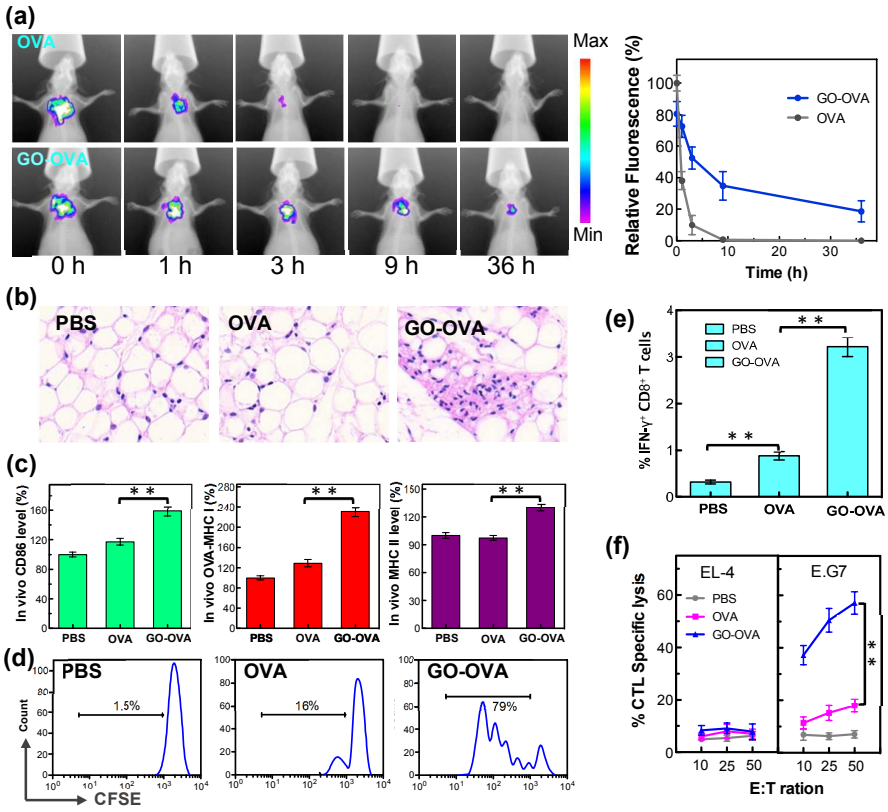

Fig. 5. In vivo validation of the adjuvanticity effect of GO. (a) Comparison of the Cy5-OVA distribution with or without GO after subcutaneous administration in the hindneck of C57BL/6 mice. Antigen fluorescence in OVA group at 0 h was normalized as 100%. (b) Hematoxylin and eosin (H&E) staining of the APCs recruitment in mice immunized with GO-OVA. (c) Improved activation of lymph node DCs after GO-OVA vaccination. (d) CFSE proliferation profile of OVA specific CD8+ T (OT-1) after antigenic immunization. Numbers in the FACS histogram represent the percentages of proliferated OT-1 cells showing a diluted CFSE content. (e) Frequency of IFN-γ+ secreting CD8 T cells in mice immunized with antigen formulations. Average percentage of the CD8 T was calculated from three independent experiments. (f) OVA-specific cytotoxic activity of spleen CTL from immunized mice E.G7 cells (with OVA gene) or EL-4 cells (without OVA gene) were used as targets. Data represent the mean±s.d. (n=3, *p<0.05, **p<0.01).

observing the histological tumor section. To gain a deep insight, we analyzed the frequency of OVA-specific CD8 T cells and revealed that the OVA-specific CD8 T cells infiltrated into tumor cells at a higher level after GO-OVA treatment (Fig. 6e). An analogous trend was also observed in the draining lymph nodes and spleen (Fig. S7†). In addition to the CD8 T mediated cellular response, the GO-OVA vaccine even elicited a strong and durable OVA-specific IgG response (Fig. S8†), which would be favorable to neutralize the circulating tumor cells. Such an orchestration of cellular and humoral response was beneficial for the efficient inhibition of tumor metastasis (Fig. S9†).

Having demonstrated the therapeutic potentials, we evaluated the health condition of tumor-bearing mice after vaccination. Blood samples were collected before scarification on day 24, and most of the vital biomedical parameters were abnormally elevated with the burden of tumor. Nevertheless, the enhanced levels of serum aspartate aminotransferase (AST), LDH, and alanine aminotransferase (ALT) that caused by tumor growth were diminished and recovered to normal ranges for the GO-OVA groups (Table S1†). These data reflected that the treatment with GO based vaccine effectively protected the mice from hepatic or other organ failure, helping maintain at a much better health condition.

Safety evaluation of GO-based vaccine

The impact of GO on cell viability has been systematically investigated in our previous study, and the asprepared GO did not exert noticeable toxicity to cells of different types.[17] For further confirmation, we continued to estimate the safety of the GO-based vaccine on animal level. When normal mice were immunized with GO-OVA for 24 days, the levels of the vital biochemical markers (LDH, blood urea nitrogen BUN, ALT, AST, and alkaline phosphatase ALP) were tested and all turned out to fall in normal ranges (Table S2†). Moreover, no obvious

inflammatory infiltrates or toxicity were observed in the histological sections of the heart, liver, lung, and kidney (Fig. S10†). Therefore, both the biochemical and histological evaluations indicated the excellent in vivo biosafety of the present GO-based vaccine. Such a satisfactory result could be partly attributed to the good biocompatibility of GO carrier. Besides, the well-limited use of GO in virtue of the high antigen loading capacity is also believed to play a beneficial role in safety aspect. The minimal demand of GO carrier could further warrant the safety of the current vaccine formulation if any possible but undiscovered GO-related side effect exists.

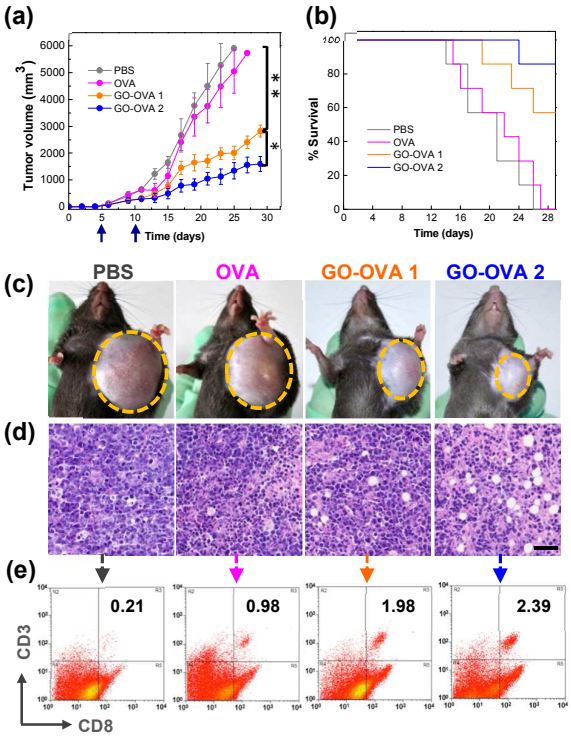

Fig. 6. Tumor therapy effect of GO adjuvanted vaccine. (a) Tumor growth volumes and survival rate (b) of mice bearing E.G7 tumors after different vaccination. (c) Representative photos of tumor-bearing mice after different treatment. (d) H&E stained images of tumor sites from vaccine treated mice. Mononuclear cells transferred into the tumor sites, and obvious cavities were formed during the tumor regression. Scale bar 50 μm. (e) FACS plots showing the infiltration of CD8 T at the tumor sites. (n=7, *p<0.05, **p<0.01).

Conclusions

In the present work, we developed a multifunctional cancer vaccine in a simple and practical way, without any extra addition of bio or chemical stimulators. The acquired effects (improved cell recruitment, antigen delivery, and antigen cross-presentation to CTL) were derived from the unique bio- or physiochemical properties of the two-dimensional material

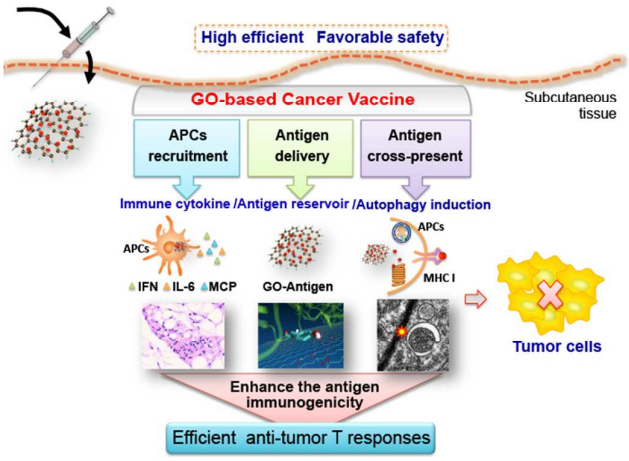

Fig. 7. A scheme of "One but All" modality of the GO-based cancer vaccine.

GO (Fig. 7). GO was an ideal platform for high antigens loading multilayer through a complex of mechanisms, with the electrostatic attractions being the dominant force. Once vaccinated, the self-produced cytokines upon GO stimulation recruited large amount of APCs to the injection sites. Following efficient cellular uptake, the flat GO was inclined to become folding shape in the APCs, thereby inducing the autophagy process and "antigen reservoir" role, which subsequently contributed to the programmatic activation of specific CD8 T cells in vivo. In terms of all the above enhancements seen with the GO adjuvant, the cytotoxic lysis activity against antigen-specific tumor cells was eventually gained, resulting in further tumor rejection. Such an unadorned but intelligent "One but All" vaccine renewed the knowledge of biological performance that based on the non-spherical biovehicle.

Although a promising avenue for developing safe and high-performance vaccine was opened, future work is still awaited. One focal point is to compare our platform with other adjuvants and further vote the feasibility for cancer vaccine. Moreover, we will utilize well-documented tumor antigens and testify the performances on corresponding malignant tumor models. In addition, the dosage and frequency of vaccination should be further systematically optimized to achieve high-performance use in practice.

Acknowledgements

This work was supported by Youth Innovation Promotion Association, CAS (2013033), 973 Program (2013CB531500), National High Technology Research and Development Program of China (2014AA093604), National Natural Science

Foundation of China (51302265, 11374221) and Major Project of the Ministry of Science and Technology of China (2014ZX09102045). RZ acknowledges the support from the IBM Blue Gene Science Program. A Project partially funded by the Priority Academic Program Development of Jiangsu Higher Education Institutions (PAPD).

Notes and references

1 P. Fernandez-Ortega, M. T. Caloto, E. Chirveches, R. Marquilles, J. S. Francisco, A. Quesada, C. Suarez, I. Zorrilla, J. Gomez, P. Zabaleta, G. Nocea and A. Llombart-Cussac, *Support Care Cancer*, 2012, **20**, 3141-3148.
2 F. Roila, J. Herrstedt, M. Aapro, R. J. Gralla, L. H. Einhorn, E. Ballatori, E. Bria, R. A. Clark-Snow, B. T. Espersen, P. Feyer, S. M. Grunberg, P. J. Hesketh, K. Jordan, M. G. Kris, E. Maranzano, A. Molassiotis, G. Morrow, I. Olver, B. L. Rapoport, C. Rittenberg, M. Saito, M. Tonato and D. Warr, *Ann Oncol*, 2010, **21 Suppl 5**, v232-243.
3 M. S. Ahmed and Y. S. Bae, *Clin Exp Vaccine Res*, 2014, **3**, 113-116.
4 S. D. Xiang, K. Scalzo-Inguanti, G. Minigo, A. Park, C. L. Hardy and M. Plebanski, *Expert Rev Vaccines*, 2008, **7**, 1103-1119.
5 K. Palucka and J. Banchereau, *Immunity*, 2013, **39**, 38-48.
6 S. Y. Liu, W. Wei, H. Yue, D. Z. Ni, Z. G. Yue, S. Wang, Q. Fu, Y. Q. Wang, G. H. Ma and Z. G. Su, *Biomaterials*, 2013, **34**, 8291-8300.
7 L. Brannon-Peppas and J. O. Blanchette, *Adv Drug Deliv Rev*, 2012, **64**, 206-212.
8 K. Sehgal, K. M. Dhodapkar and M. V. Dhodapkar, *Immunol Lett*, 2014.
9 H. L. Jiang, M. L. Kang, J. S. Quan, S. G. Kang, T. Akaike, H. S. Yoo and C. S. Cho, *Biomaterials*, 2008, **29**, 1931-1939.
10 O. A. Ali, N. Huebsch, L. Cao, G. Dranoff and D. J. Mooney, *Nat Mater*, 2009, **8**, 151-158.
11 J. T. Wilson, S. Keller, M. J. Manganiello, C. Cheng, C. C. Lee, C. Opara, A. Convertine and P. S. Stayton, *ACS Nano*, 2013, **7**, 3912-3925.
12 Z. Cheng, A. Al Zaki, J. Z. Hui, V. R. Muzykantov and A. Tsourkas, *Science*, 2012, **338**, 903-910.
13 L. Feng, L. Wu and X. Qu, *Adv Mater*, 2013, **25**, 168-186.
14 K. Yang, L. Z. Feng, X. Z. Shi and Z. Liu, *Chem Soc Rev*, 2013, **42**, 530-547.
15 W. Miao, G. Shim, S. Lee, S. Lee, Y. S. Choe and Y. K. Oh, *Biomaterials*, 2013, **34**, 3402-3410.
16 Z. Yue, P. Lv, H. Yue, Y. Gao, D. Ma, W. Wei and G. Ma, *Chem Commun (Camb)*, 2013, 49, 3902-3904.
17 H. Yue, W. Wei, Z. Yue, B. Wang, N. Luo, Y. Gao, D. Ma, G. Ma and Z. Su, *Biomaterials*, 2012, 33, 4013-4021.
18 C. Ge, J. Du, L. Zhao, L. Wang, Y. Liu, D. Li, Y. Yang, R. Zhou, Y. Zhao, Z. Chai and C. Chen, *Proc Natl Acad Sci U S A*, 2011, 108, 16968-16973.
19 Y. Tu, M. Lv, P. Xiu, T. Huynh, M. Zhang, M. Castelli, Z. Liu, Q. Huang, C. Fan, H. Fang and R. Zhou, *Nat Nanotechnol*, 2013, 8, 594-601.
20 R. Zhou, X. Huang, C. J. Margulis and B. J. Berne, *Science*, 2004, 305, 1605-1609.
21 C. M. Hu, S. Kaushal, H. S. Tran Cao, S. Aryal, M. Sartor, S. Esener, M. Bouvet and L. Zhang, *Mol Pharm*, 2010, 7, 914-920.
22 D. F. Emerich and C. G. Thanos, *J Drug Target*, 2007, 15, 163-183.
23 D. Stauffer, N. Dragneva, W. B. Floriano, R. C. Mawhinney, G. Fanchini, S. French and O. Rubel, *J Chem Phys*, 2014, 141.
24 Z. Yang, Z. Wang, X. Tian, P. Xiu and R. Zhou, *J Chem Phys*, 2012, 136, 025103.
25 G. Zuo, S. G. Kang, P. Xiu, Y. Zhao and R. Zhou, *Small*, 2013, 9, 1546-1556.
26 G. Zuo, X. Zhou, Q. Huang, H. P. Fang and R. H. Zhou, *J Phys Chem C*, 2011, 115, 23323-23328.
27 A. Lerf, H. Y. He, M. Forster and J. Klinowski, *J Phys Chem B*, 1998, 102, 4477-4482.
28 C. Gomez-Navarro, J. C. Meyer, R. S. Sundaram, A. Chuvilin, S. Kurasch, M. Burghard, K. Kern and U. Kaiser, *Nano Lett*, 2010, 10, 1144-1148.
29 A. Ganguly, S. Sharma, P. Papakonstantinou and J. Hamilton, *J Phys Chem C*, 2011, 115, 17009-17019.
30 G. Y. Chen, H. J. Yang, C. H. Lu, Y. C. Chao, S. M. Hwang, C. L. Chen, K. W. Lo, L. Y. Sung, W. Y. Luo, H. Y. Tuan and Y. C. Hu, *Biomaterials*, 2012, 33, 6559-6569.
31 M. Uhl, O. Kepp, H. Jusforgues-Saklani, J. M. Vicencio, G. Kroemer and M. L. Albert, *Cell Death Differ*, 2009, 16, 991-1005.
32 H. Y. Li, Y. H. Li, J. Jiao and H. M. Hu, *Nat Nano*, 2011, 6, 645-650.
33 V. L. Crotzer and J. S. Blum, *Immunology*, 2010, 131, 9-17.
34 T. W. Flinsenberg, E. B. Compeer, J. J. Boelens and M. Boes, *Clin Exp Immunol*, 2011, 165, 8-18.
35 I. A. Cockburn, Y. C. Chen, M. G. Overstreet, J. R. Lees, N. van Rooijen, D. L. Farber and F. Zavala, *Plos Pathog*, 2010, 6.